Experimental Thermal and Fluid Science 129 (2021) 110440

Contents lists available at ScienceDirect

Experimental Thermal and Fluid Science

journal homepage: www.elsevier.com/locate/etfs

Heat transfer characteristics of CO_2 condensation on common heat exchanger materials: Method development and experimental results

Ingrid Snustad [a,*], Åsmund Ervik [b], Anders Austegard [b], Amy Brunsvold [b], Jianying He [a], Zhiliang Zhang [a]

[a] Faculty of Engineering, Department of Structural Engineering, Norwegian University of Science and Technology, Richard Birkelands vei 1A, 7491 Trondheim, Norway
[b] SINTEF Energy Research, Sem Sælands vei, 117034 Trondheim, Norway

ARTICLE INFO

Keywords:
Condensation heat transfer
Roughness dependent heat transfer
CO_2 liquefaction
Surface roughness
Nusselt model

ABSTRACT

Understanding condensation of CO_2 is essential for e.g designing compact heat exchangers or processes involved in Carbon Capture and Storage. However, a consistent experimental campaign for condensation of CO_2 on common materials is lacking. In this work, we present an experimental method and an associated laboratory setup for measuring the heat transfer properties of CO_2 condensation on materials commonly used in heat exchangers for the liquefaction of CO_2. We have investigated the heat transfer during CO_2 condensation on copper, aluminum, stainless steel (316) to reveal the heat transfer dependency on surface properties. The experiments are conducted at three saturation pressures, 10, 15, and 20 bar and at substrate subcooling between 0 and 5k. The results show that the heat transfer coefficients decrease with increasing surface subcooling. It was also found that increasing the saturation pressure increases the heat transfer coefficient. The results indicate that surface roughness and surface energy affect the condensation heat transfer coefficient, and an increased roughness results in reduced heat transfer coefficients. The highest heat transfer coefficient is found for condensation on copper, for which the lowest surface roughness has been measured.

1. Introduction

Condensation of CO_2 occurs in several stages of industrial processes. The need for eliminating fluorine based refrigerants due to their environmental impact has, for example, opened up for CO_2 as an alternative cooling fluid in heat exchangers. The global warming potential of CO_2 is about three orders of magnitude lower than for the traditional refrigerants [1]. CO_2 has a high triple point pressure and low critical pressure, which makes it suitable for use in cooling systems. Another example is the use of CO_2 as a refrigerant in compact heat exchangers, such as in motor vehicle air-conditioning [2]. Heat exchangers with CO_2 as the refrigerant or designed for liquefaction of CO_2 are commonly made of e.g. copper (Cu), aluminum (Al) or stainless steel (steel) [2–4].

CO_2 condensation is also a pre-process for CO_2 transport during Carbon Capture and Storage (CCS). CO_2 is emitted on a large scale, and in some industries, such as cement and aluminum production, CCS is the only solution for mitigating the emissions [5]. CO_2 is mainly transported via pipeline or ship. Cost assessments of CO_2 transportation show that for long distances and/or small amounts, ship transport is the preferred solution over pipeline. In this case, the CO_2 will be transported in the liquefied state at about -55 °C and 5-SI7 bar [6–10], but other options are being investigated. Reducing the energy demand of the liquefaction process will play a key role in reducing costs of ship transportation. As a result, a thorough understanding of every aspect regarding CO_2 condensation is necessary for proper process design and ultimately for reducing energy needs and costs for CO_2 condensation.

Previous studies on CO_2 condensation have focused on the flow condensation heat transfer coefficient (HTC) in various geometries, especially tubes and channels with varying diameter, from micro to macro scale [11–15]. The heat transfer properties are, in these cases, particularly affected by the flow pattern and the surface roughness internally in the channels. The well known and widely used Nusselt model for filmwise condensation on flat surfaces [16,17] is an idealized analytical model that does not include surfce roughness or other substrate specific properties. For dropwise condensation heat transfer a low thermal conductivity increases the constriction resistance, thereby reducing the HTC [18]. For filmwise condensation, such material specific properties will not influence the condensation heat transfer

* Corresponding author.
E-mail address: ingrid.snustad@ntnu.no (I. Snustad).

https://doi.org/10.1016/j.expthermflusci.2021.110440
Received 10 December 2020; Received in revised form 15 April 2021; Accepted 13 May 2021
Available online 1 June 2021
0894-1777/© 2021 The Author(s). Published by Elsevier Inc. This is an open access article under the CC BY license (http://creativecommons.org/licenses/by/4.0/).

resistance. Surface properties, such as roughness and surface energy, will, however, influence the heat transfer. In response to the absent studies on CO_2 condensation heat transfer on various vertical surfaces, we here report a comparison of the heat transfer performance of Al, Cu, and steel under the condensation of CO_2.

As stated above, surface roughness may play an important role in the condensation process [19], and controversial results about the effect of roughness on heat transfer have been reported. For example both Soontarapiromsook et al. [20] and Nilpueng et al. [21] observed that condensation HTC increases with surface roughness, while Yun et al. [22] came to the opposite conclusion. For this reason, we have investigated the influence of surface roughness on condensation. Modification of the surface caused by the condensation itself, may also affect the heat transfer. In particular, CO_2 adsorption on Cu has been studied in the literature, with focus on Cu as a catalyst in reactions involving CO_2, e.g. methanol synthesis [23]. Muttaqien et al. [24] concluded that CO_2 in the gaseous state does not dissociate on clean Cu at low temperatures. CO_2 in the liquid state has, however, not been studied, and the interaction between liquid CO_2 and Cu is not understood. The formation of liquid CO_2 on Cu and the effect on the HTC will be briefly discussed in this work.

Experimentally determining the HTC in CO_2 condensation is challenging, and no previous study has reported the condensation HTC of CO_2 on flat surfaces. In this study, for the first time, an experimental method that can accurately measure the static condensation HTC of CO_2 is developed. The experimental setup is built for a straightforward alternation between substrates, and systematic studies of the heat transfer on samples with a variety of surface properties and surface modifications can be performed. With the established method, the heat transfer during condensation of CO_2 on the aforementioned materials, Cu, Al, and steel, have been investigated. The condensation is studied at saturation pressures of 10 bar, 15 bar and 20 bar and surface subcooling between 0k and 5k. The surface subcooling is defined as the difference between the saturation temperature, T_{sat}, and the surface temperature, T_{surf}.

In the following, the experimental method developed especially for condensing CO_2, including the detailed setup, an overview of the piping and instrumentation diagram (P&ID), the data acquisition and reduction rules adopted, is presented first. The theoretical principles governing the development of the experimental method are documented in the Supplementary Information. In Section 3 an overall description of the three investigated materials is reported. In Section 4, the experimental results, in particular, the surface roughness dependence of the measured HTC and the unique CO_2 adsorption behavior on Cu, are elaborated. Some concluding remarks as well as topics suggested for future research to improve the experimental method and understanding of the heat transfer in CO_2 condensation are presented in Section 5.

2. Methodology

The experimental method for determining the heat transfer properties of various materials developed in this work, will be described in this section. The method is based on the theory of one-dimensional heat transfer through a Cu cylinder (Fourier theory) [25,26]. The methodology is outlined through a description of the experimental setup and an explanation of the data acquisition and reduction through a presentation of the necessary equations.

2.1. The experimental setup

The specially designed parts of the experimental setup are the pressure chamber, the cooling element and a gas delivery system for both liquid CO_2 for cooling and clean gaseous CO_2 to be condensed. In addition, the setup is equipped with a high speed camera (Phantom 9.1) for observing the point of condensation and to what extent the condensation has developed. The design of the setup, including all tubes, pipes, valves and larger components, is presented as a P&ID, shown in Fig. 1. The descriptions of the components in the following sections should be referred to the P&ID.

2.1.1. The pressure chamber and gas delivery system

Condensation of CO_2 will never occur in an atmospheric environment. The thermodynamic triple point of CO_2 is at 5.2 bar and -56.6 °C, requiring a pressurized chamber in which the vapor will condense. The pressure level for ship transport of CO_2 will be in the same order of magnitude as the triple point [7], and the pressure chamber is therefore designed and fabricated for pressures up to 20 bar. The chamber is a stainless steel pipe (diameter $= 20$cm, length $= 30$cm) with 10 sealed holes in the pipe wall. These are included for gas inlet and outlet, cooling fluid inlet and outlet, pressure sensors, thermal measurements and a custom made electrical cable feedthrough. Swagelok couplings are used for ensuring pressure-tight inlets and outlets. The electrical cable feedthrough is a 16 mm OD tube in which wires for four T-type thermocouples (TCs) and LED lights is embedded in two component epoxy. The epoxy was fed into the tube at elevated temperature in two steps. The feedthrough was tested at 25 bar helium for which no detectable leakage was present. If additional light sources or other electrical cables are needed, an alternate feedthrough could easily be replaced with the current version. The chamber and the high speed camera are shown in Fig. 2.

The lid in the front, facing the camera, is a double flange with a sight glass embedded in the center. On the inside of the sight glass, a strip of LED light is attached around the circumference, see Fig. 3. As a result, the surface to be examined is lit from all sides during experiments.

Condensation of humid air and ice formation onto the sight glass will disturb the imaging of the condensation process. Therefore, it is necessary to reduce the dew point below the experimental temperature. For this reason, the experiments are performed at a surrounding temperature of around -10 °C and in a dry environment. The temperature is provided by lowering the pressure chamber and the camera into a freezer (Scandomestic SB 650). A hose with pressurized and dried air is inserted into the freezer through a drilled hole. The air will provide the necessary low humidity environment in the freezer. The air is dried with a Kaeser DC 4.2 air dryer. At -10 °C and 5% relative humidity, which are typical parameters of the setup, the dew point is -42 °C. The temperature inside the pressure chamber is set by the freezer temperature, so the temperature on the outside of the sight glass will be well above the dew point temperature, as required, and the see glass will be free of ice.

During operation, the chamber is filled with pressurized, gaseous CO_2. A gas delivery system consisting of a gas cylinder (Scientific CO_2, 6.0 purity, AGA) and a differential pressure controller (Alicat PCD) fills the chamber to the saturation pressure determined by the operator. According to previous reports, non-condensable gases and humidity will alter the heat transfer characteristics of the condensation [27–29]. The chamber is therefore vacuumised and flushed with CO_2 in three cycles before filling to the desired pressure. A vacuum pump is used to empty the chamber down to < 0.1mbar, between each flushing of 1 bar CO_2.

2.1.2. The cooling element

If condensation is to occur on the investigated surfaces, they must be cooled below the saturation temperature of the vapor. A stable temperature down to -55 °C is the target, for which condensation of CO_2 will occur if the pressure in the vapor is above 5.6 bar. In order to achieve the low temperatures, a small heat exchanger is designed and fabricated for cooling the investigated surfaces with a high degree of temperature stability, uniformity and control. The cooling element consists of a rectangular block of Cu where the bottom and the sides are insulated with a layer of insulation foam. Within the block there are narrow parallel channels, see Fig. 4, in which the refrigerant will flow. A CO_2 gas cylinder with a liquid riser is coupled to the cooling circuit. Initially, pressurized gaseous CO_2 flows in the circuit, followed by an increase in

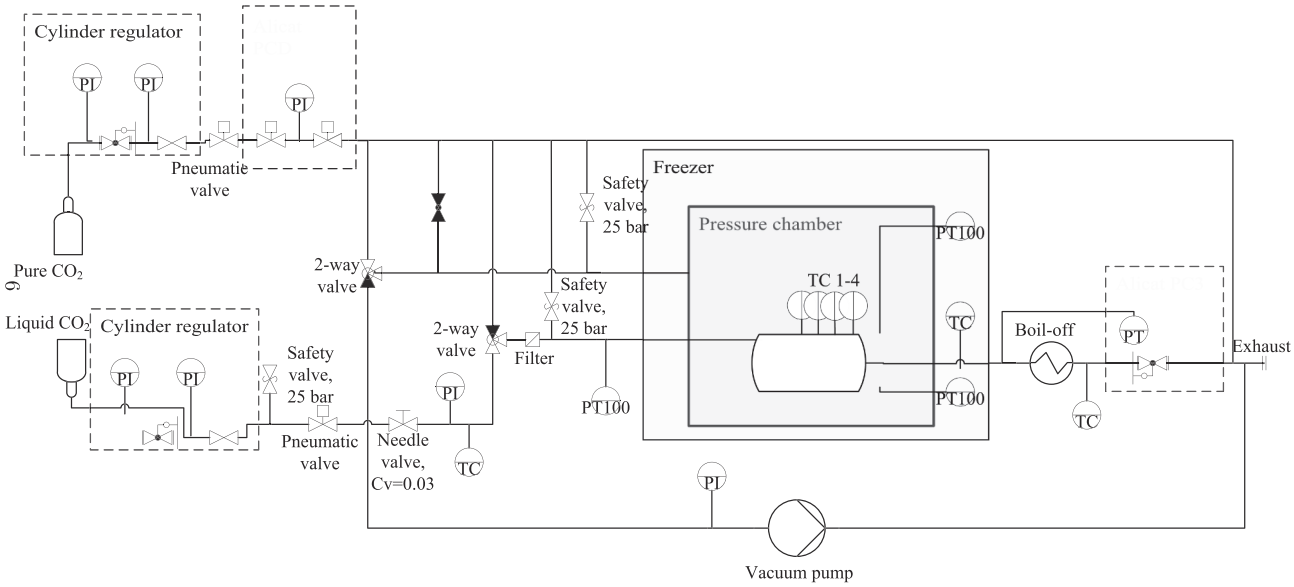

Fig. 1. Piping and Instrumentation Diagram of the experimental setup. Pure CO_2 flows into the pressure chamber with the Alicat PCD as the pressure controller. Liquid CO_2 is fed to the cooling element with the Alicat PC3 as a back pressure regulator, accurately controlling the pressure which results in a uniform temperature in the cooling element.

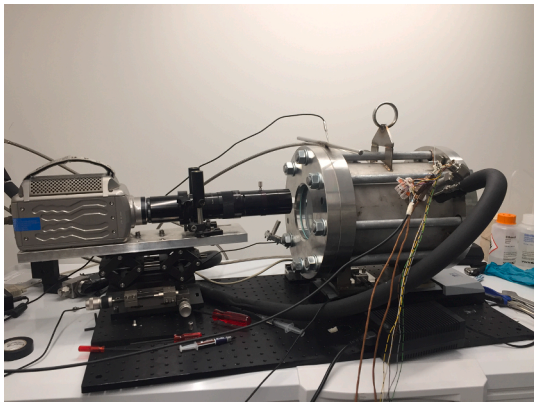

Fig. 2. The pressure chamber consists of a steel cylinder (20cm diameter) with two flanges as lids. 8 bolts keep the flanges together and two O-rings embedded in the flanges seal the chamber against leakage. A high-speed camera (Phantom 9.1) is placed in front of the chamber to monitor condensation through the sight-glass.

pressure and mass flow until they are high enough to realize two-phase flow through the heat exchanger. The pressure is set to the saturation pressure corresponding to the desired temperature, and the mass flow is adjusted with a needle valve until two-phase is obtained. The saturation pressure is varied between 6 and 20 bar, in the current design. The pressure in the circuit is controlled by a back pressure regulator (Alicat PC3). We know that two-phase flow is obtained when a TC embedded in the flow upstream the cooling element (marked TC downstream the Needle valve in the P&ID, Fig. 1) suddenly drops to the desired cooling temperature. When two-phase flow is obtained in the entire circuit, the desired temperature is observed in the TC that is embedded in the tube downstream the cooling element. Two-phase CO_2 will flow and convective boiling will occur in the channels of the cooling element. By adjusting the volumetric flow of the liquid CO_2 entering the heat exchanger, and accurately controlling the pressure drop through the cooling element, it is possible to ensure that there is two-phase flow at the outlet of the heat exchanger, and hence, that the temperature across the cooling element surface is uniform.

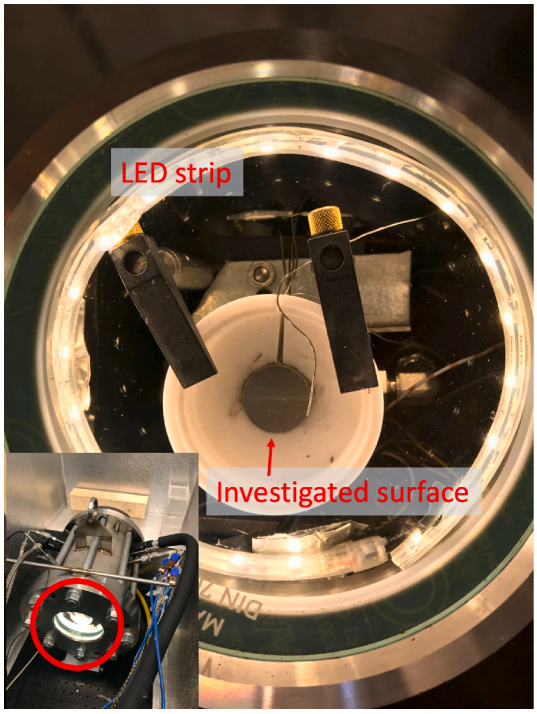

Fig. 3. View of the investigated surface through the sight glass in the lid. The red ring in the inset shows where the sight glass is located in the pressure chamber. A strip of LED light is fastened around the inner circumference of the glass and the surface is lit from all sides during experiments.

2.2. Data acquisition and reduction

The pressure and temperature measurements are collected and visualized by a LabVIEW^{TM} program. Through the LabVIEW^{TM} program the user can set the correct temperature of the cooling block, the desired saturation pressure and record the output from the TCs, PT100s and pressure measurements. The measurement data are reduced according to the following calculations.

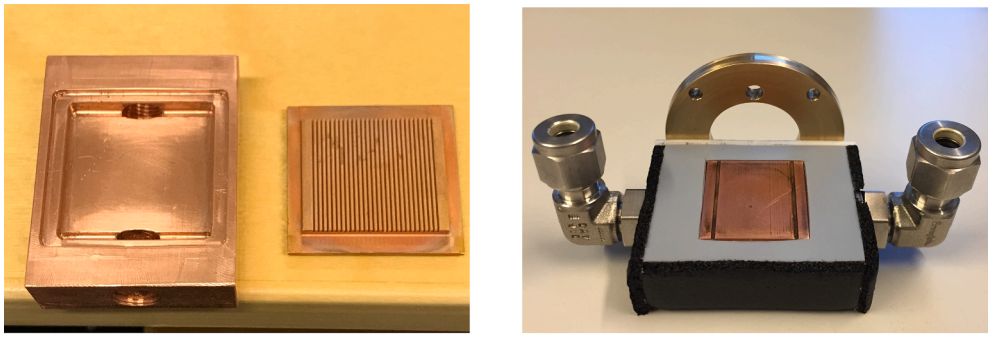

(a) (b)

Fig. 4. (a) The interior of the cooling element, which consists of a Cu slab with narrow channels for accurate control of surface temperature. (b) The assembled cooling element with inlet and outlet for two phase flow.

$$q_{tot} = -k\nabla T \tag{1}$$

The total heat flux is calculated with the Fourier heat flux equation in Eq. (1). Here, ∇T is the temperature gradient through the Cu cylinder and k is the thermal conductivity of Cu. The temperature gradient is found by linear regression of the temperatures in the four TCs embedded in the center of the Cu cylinder. The thermocouples are of T-type and are "on site" calibrated in an icebath, i.e. the thermocouples were embedded in the Cu cylinder, and all other connections were as they were in an experiment, see Supplementary Information. Since the temperature profile is linear the gradient becomes $\nabla T = \frac{dT}{dx}$. The linearity of the gradient is confirmed by the detailed calculations included in the Supplementary Information.

The condensation heat flux is calculated by subtracting the heat flux for cooling the gas in the pressure chamber, q_{gas}, and the heat that is lost through the Teflon insulation, q_{teflon}, from the total heat flux in Eq. (1), resulting in Eq. (2).

$$q_{cond} = q_{tot} - q_{gas} - q_{teflon} \tag{2}$$

q_{gas} is calculated with Eq. (3). The gas temperature, T_{gas}, has been measured for the three investigated saturation pressures at all levels of subcooling, and an average value of q_{gas} for each pressure is used in the calculation of q_{cond}. Mm and c_p are the molar mass and heat capacity of CO_2 at the gas temperature, while A is the surface area of the investigated sample.

$$q_{gas} = c_p Mm(T_{gas} - T_{sat})/A \tag{3}$$

$$h_c = \frac{q_{cond}}{T_{sat} - T_{surf}} \tag{4}$$

The condensation HTC, h_c, is defined by Eq. (4). The temperature in the saturated vapor adjacent to the condensate, T_{sat}, is calculated with the Span–Wagner Equation of State [30] (calculated with the NIST Webbook [31]), at the set pressure in the chamber. The surface temperature, T_{surf}, is calculated by the following procedure. First, the surface temperature of the Cu cylinder is extrapolated from the temperature measurement data. Second, using the constant heat flux, the Fourier equation (Eq. (1)) is used to calculate the gradient in the thermal interface material (TIM), which attaches the samples to the cylinder. As a result, the temperature at the interface between the TIM and the investigated material is found. Finally, the heat flux and Fourier equation is used to calculate the temperature gradient in the investigated material, with thermal conductivity, k, for the specific material. The surface temperature is calculated with the gradient in each investigated material. Fig. 5 shows an example of the temperature measurements, the linear regression and the resulting cylinder surface temperature.

The experimental data confirm that the temperature gradient

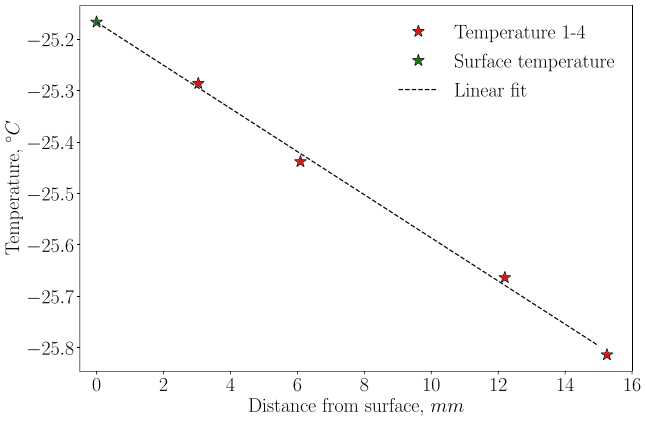

Fig. 5. Average temperatures in the four thermocouples embedded in the Cu cylinder, for one pressure and one subcooling. The linear fit provides the gradient of the temperatures, and hence the total heat flux through the cylinder. The fit also enables the calculation of the surface temperature by extrapolation, shown by the green star.

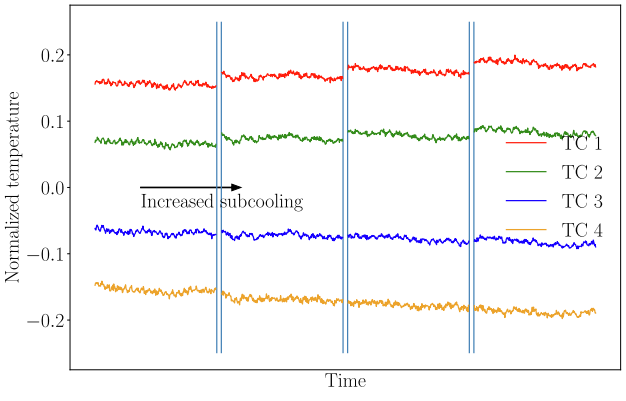

Fig. 6. Experimental measurements of the temperature in the cylinder at the position of the four embedded thermocouples, with TC 1 closest to the cooling element. The difference between TC 1 and TC 4, and hence the temperature gradient, increases for increased subcooling. The average value of the four thermocouples are subtracted in each point in order to visualize the increase of the gradient. The vertical lines divide the measurements into one area for each level of subcooling. Each vertical line represent a small jump in time (time for stable temperatures after changing subcooling).

through the cylinder increases for increasing subcooling of the surface, shown in Fig. 6. The figure includes 300 measurement points per thermocouple per level of subcooling, and four levels of subcooling. The vertical lines marks the transition between two levels of subcooling, i.e. a new temperature setpoint in the cooling element. At each vertical lines there is a time step, with the time it takes for the temperatures to stabilize.

Fig. 7 shows the scattering of the temperature measurements in the four TCs in the cylinder. The data are recorded at three different levels of subcooling (red, green and blue), and at a saturation pressure of 15 bar. The TCs are placed at approximately 3, 6, 12 and 15mm from the cylinder surface. The temperature of the fitted point for the TC at 3mm (denoted T(1) in the Figure) is subtracted from all points for a clearer comparison of the values. Each blob of red, green and blue consists of 300 measurement points and their spread in the vertical direction equals the temperature scattering for each measurement. This experimental scattering is maximum 0.03k.

2.3. Uncertainties

Table 1 presents the values of uncertainty that have been used for estimating the errors in the presented data. An uncertainty analysis has been carried out based on Gaussian error propagation, and the formulas are included in the Supplementary Information. The uncertainty in the thermocouple measurements, $TC1 - TC4$, is estimated from the relative deviation of the icebath calibration (details in Supplementary Information) and the variation in the 300 measurement points taken for each measurement, as shown in Fig. 7. The uncertainty in P_{sat} is given by the specifications of the Alicat PCD pressure sensor, and it is used to calculate the uncertainty in T_{sat}. For T_{surf}, we have estimated the uncertainty based on the uncertainty in the thickness of the thermal interface material, t_{TIM}, and the propagation of the errors in the extrapolation process. The estimated errors in heat flux, E_q, will propagate to the calculated values of HTC as well. However, as the definition of HTC includes $T_{sat} - T_{surf}$ in the denominator, the propagated errors will increase to infinity for small subcooling. The errorbars in HTC are therefore excluded in the results, Fig. 10.

3. Materials

Three materials commonly used in process equipment, especially where condensation occurs, have been investigated. These are Cu, Al, and steel. The substrates were circular discs, 2cm in diameter, which were cut from rolled plates. The thickness of Cu and steel were 0.5mm,

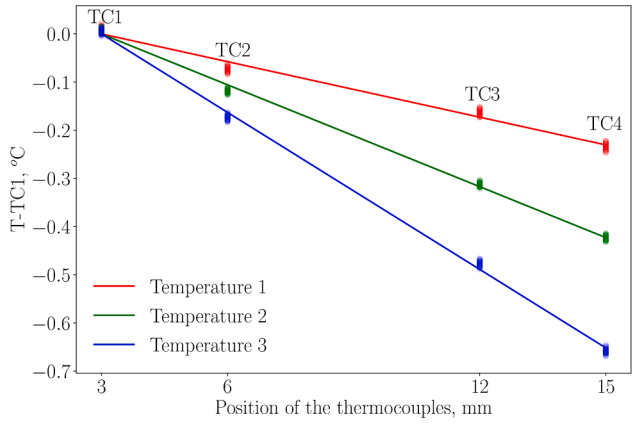

Fig. 7. Three representative temperature measurements in the four thermocouples embedded in the core of the Cu cylinder. The temperature in TC1 is subtracted from each measurement point and the positions of the thermocouples are given relative to the surface of the investigated material. The scattering of the measurements (width of the blobs) are 0.03k.

Table 1
Table with the estimated uncertainties used for calculating the overall uncertainties in heat flux and subcooling.

Parameter	Uncertainty name	Uncertainty value
TC_1, TC_2, TC_3, TC_4	E_T	±0.0337k
P_{sat}	n/a	±0.0875 bar
T_{sat}	$E_{T_{sat}}$	±0.2k
t_{TIM}	$E_{t_{TIM}}$	±0.05mm
k_{Cu}	$E_{k_{Cu}}$	±0.013% [32]
k_{mat}	$E_{k_{mat}}$	±5%
$x_4 - x_1 = d_{1-4}$	$E_{d_{14}}$	±0.04mm
x_1	E_{x_1}	$E_{d_{14}}/2$

while Al was 0.7mm. The surface roughness has been measured for all surfaces with a Veeco Dektak 150 Profilometer. Ten line scans, each 5μm in length, have been performed for each surface, and the results presented in Table 2 are the average values of the ten scans. The Al surface has the highest roughness, while the Cu surface is least rough, in terms of arithmetic mean average (MA) roughness and root mean square (RMS) roughness. (see Table 3).

The investigated substrates were cleaned with acetone, isopropanol and ethanol, and subsequently dried with pressurized dry air. The substrates were then attached to the Cu cylinder with a TIM (Aldrich Chemistry, Silver Conductive paste 735825). The TIM was applied in a thin uniform layer covering the entire cylinder end surface. The investigated substrate was pressed onto the surface, resulting in that the TIM spread uniformly under the investigated substrate. The thickness of the TIM has been measured to be approximately 0.15mm with an estimated error of ±0.05mm. The thickness was measured with a caliper by applying a layer of TIM on a detached circular disc with the same application technique. The Cu cylinder was fabricated in a lathe.

4. Results and discussion

4.1. Verification of setup

To ensure that no systematic error appears caused by the attachment of substrates to the Cu cylinder, we have conducted condensation experiments on the cylinder without any attached substrate. In Fig. 8 condensation heat flux obtained on the bare Cu cylinder are plotted together with the heat flux data obtained on the attached Cu substrate. The condensation heat fluxes are well within the experimental uncertainties, and as a result we conclude that the procedure of attaching the samples to the cylinder surface does not affect the heat transfer behavior. In the figure, theoretical heat flux calculated with the Nusselt model is also plotted. We see that the experimental data lies within a 15% deviation from the theoretical values. The deviation from the theoretical values is expected as the Nusselt model is idealized and does not consider surface properties of the material, vapor drag, or non-laminar flow. (see Fig. 9).

Table 2
MA and RMS roughnesses of the investigated surfaces, along with typical values for the surface energies. The surface energy for the aluminum sample is given for Al_2O_3 as an Al surface in atmospheric environment will be oxidized.

Material	MA	RMS	Peak-to-valley	Surface
	Roughness (nm)	Roughness (nm)	Roughness (nm)	Energy (mJ/m^2)
Copper	73.3	93.4	250	1650 [33]
Aluminum	513.1	722.6	2000	169 [34]
Stainless steel (316)	243.5	312.3	1000	53 [35]

Table 3
Relevant thermophysical properties of CO_2 at the two-phase line

	10 bar	15 bar	20 bar
	-40.1 °C	-28.5 °C	-19.5 °C
Liquid density, ρ_l (kgm^{-3})	1121.8	1074.2	1034.0
Vapor density, ρ_v (kgm^{-3})	26.2	39.2	52.8
Density difference, $\rho_l - \rho_v$ (kgm^{-3})	1095.6	1035.0	981.2
Viscosity, μ_l (mpa s)	2.0	1.7	1.4
Latent heat, h_{fg} (kJ kg^{-1})	320.8	300.0	281.6
Thermal conductivity, k_l ($mWm^{-1}K^{-1}$)	159.8	145.4	134.3
Surface tension, λ (mNm^{-1})	13.15	10.47	8.48

4.2. Condensation heat transfer on Cu, Al and steel surfaces

The condensation heat flux of CO_2 on Cu, Al, and steel have been measured at 10, 15, and 20 bar while varying the subcooling between 0 and 5k. The condensation heat flux increases for increasing subcooling and increased saturation pressure. The errors in heat flux and subcooling are results of the uncertainty analysis described above and in the Supplementary Information. The condensation HTCs for the three saturation pressures are shown in Fig. 10, together with the results of the Nusselt model for CO_2 condensation. For each material and pressure, the condensation HTCs approach a constant level for high subcooling. The constant level is reached for lower values of subcooling compared to the Nusselt model. Similar behavior has also been observed for filmwise steam condensation on modified titanium with high surface energy [36]. However, the mechanism of the phenomena is not yet described.

The Nusselt model is an analytical model of filmwise condensation on a vertical wall [16]. The Nusselt model for calculating the HTC, h_{Nu}, is

$$h_{Nu} = \frac{4}{3}\left(\frac{g\rho_l(\rho_l-\rho_v)h'_{fg}k_l^3}{4\mu_l L(T_{sat}-T_{surf})}\right)^{1/4}, \quad (5)$$

where g is the gravitational acceleration, h'_{fg} is the latent heat modified to compensate for thermal advection effects, following the procedure of Rohsenow [37,17], ρ_l and ρ_v are the liquid and vapor density, respectively, μ_l is the dynamic viscosity of the liquid, and L is the characteristic length of the surface, which in this case is the diameter of the Cu cylinder. Nusselt theory is derived for a rectangular surface, but previous work has shown that the deviation due to a circular surface is negligible [26]. The Nusselt model also gives a value for the condensate film thickness along the height of the surface, Eq. (6), where x is the distance from the top of the surface. The resulting CO_2 film thickness along the substrate is shown in Fig. 11.

$$\delta(x) = \left(\frac{4\mu_l k_l(T_{sat}-T_{surf})x}{g\rho_l(\rho_l-\rho_v)h'_{fg}}\right)^{1/4} \quad (6)$$

At the bottom of the surface, and at a saturation pressure of 10 bar and subcooling of 2k, the Nusselt model predicts that the film thickness of CO_2 is 34.1μm, see Fig. 11. In the figure a representation of the height of the roughness on Al (the roughest surface studied in this work) is shown, and it is clear that the predicted film thickness is thicker than the roughness of all three substrates. At low subcooling, the magnitudes of the film thickness and the roughness become close, and as a consequence it is expected that the experimental data will deviate from the Nusselt model. For very low subcooling, the film will become discontinuous across the surface, resulting in a non-uniform temperature distribution. The deviation between the Nusselt model and the experimental results increases significantly when the subcooling decreases to zero, which supports the claim that the roughness plays an increasingly important role in this case. In the Nusselt model the film thickness uniformly approaches zero for zero subcooling, and the HTC therefore approaches infinity. This is of course unphysical, and in experiments, an infinite HTC will never be found.

The experimental HTC values for subcooling above 1k and at saturation pressures 15 and 20 bar follow the same trend as the Nusselt model. The behavior of the HTC for low subcooling and for 10 bar subcooling is challenging to interpret at this moment and understanding the mechanism governing the condensation in these cases requires additional investigations.

4.3. Pressure dependence of condensation heat transfer

The condensation HTC is a pressure dependent quantity. According to the Nusselt model the HTC decreases with increasing pressure. The pressure dependence of the experimental HTC in this work is found opposite to that given by the Nusselt model, with increasing HTC for increasing pressure, shown in Fig. 13. One reason for this is the questionable validity of the laminar-flow assumption in Nusselt theory. The Nusselt model is only valid for laminar flow, and experiments have shown that for a Reynolds number, Re, above 20, this laminar flow assumption will not hold [38], and the flow will become wavy. The theoretical turning point between laminar and wavy flow for CO_2 at 20 bar will occur at a subcooling of 3.5k, and Re will continue to increase with increasing subcooling. With a wavy flow, the condensation HTC will increase, and the occurrence of wavy flow is therefore assumed to be part of the reason why the condensation HTC increases with pressure, in contrast to what Nusselt theory predicts. Another contribution to the opposite dependence on pressure is that a small error in calculated viscosity or thermal conductivity easily would switch the pressure

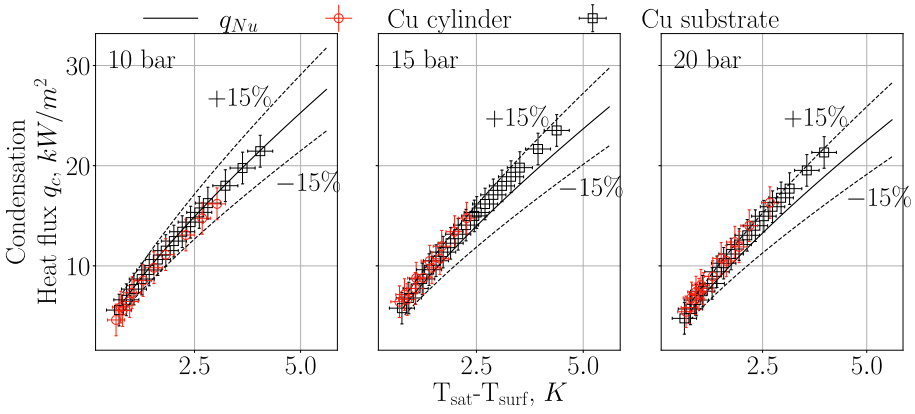

Fig. 8. Theoretical and experimental heat flux data for CO_2 condensation on the bare Cu cylinder and on the Cu substrate while attached to the cylinder with the TIM. All experimental data lies within the values of uncertainty, and within a 15% deviation from the Nusselt model.

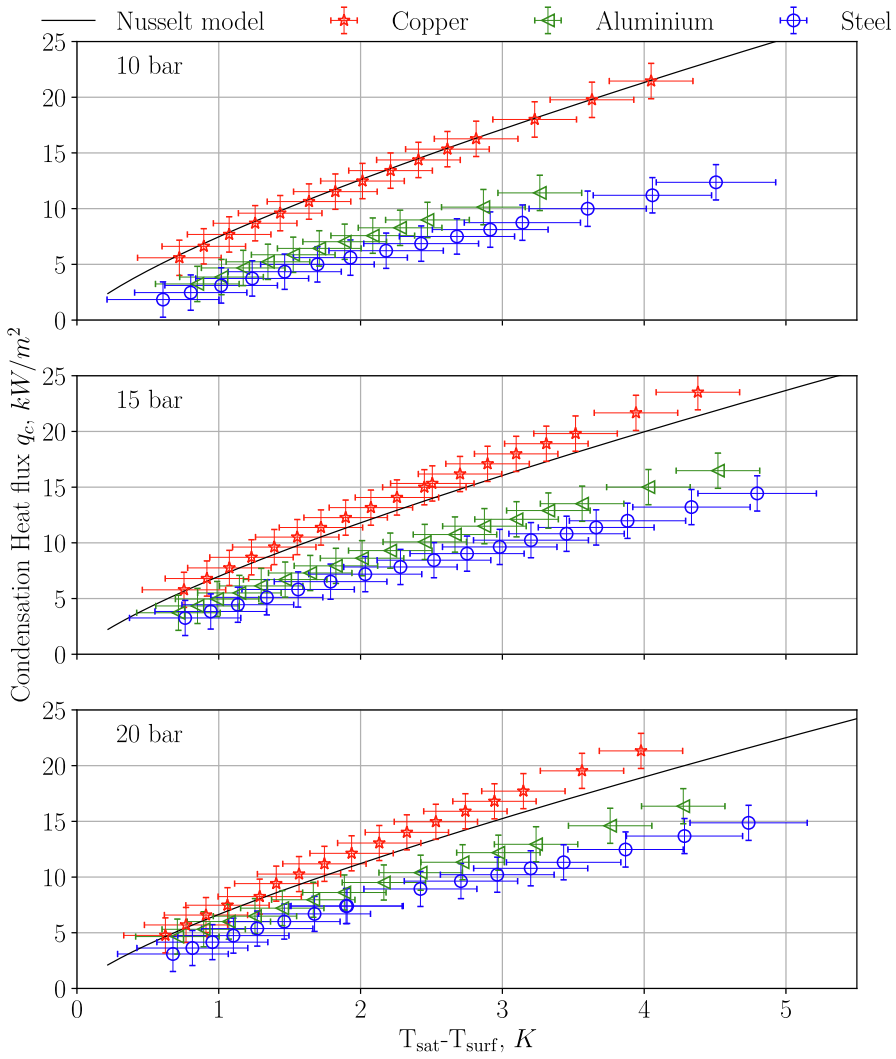

Fig. 9. Condensation heat flux for Cu, Al, and steel at 10 bar, 15 bar and 20 bar saturation pressure. The errorbars are calculated with the Gaussian error propagation shown in Supplementary Information with the uncertainty estimates in Table 1.

dependency also of the Nusselt model. The individual effects of the separate condensate properties on the HTC as modeled by Nusselt is shown in Fig. 12. We have seen that the Nusselt model does not adequately represent the heat transfer during condensation of CO_2 on the investigated samples and that the change in HTC due to pressure is smaller than the deviation between the modeled and the experimental data. The pressure dependence is not linear, and it is similar for the three substrates with a larger increase between 10 and 15 bar compared with 15 and 20 bar. The increase in HTC with pressure indicates that the film thickness is reduced for higher pressures, since the film thickness is inversely proportional to HTC. The reduction in film thickness with increased pressure may be caused by a decreased viscosity and hence a larger downward flow of the liquid due to gravity. Experimental investigation of the actual film thickness is necessary to decipher the behavior and is suggested for further work. The evolution in HTC with pressure indicates that the effects of pressure and roughness are independent.

4.4. Dependence of condenser surface properties

From the results, we see a difference in the heat flux and HTC between the three investigated samples. As stated above, the difference between steel and Al cannot be confirmed as it lies within the estimated uncertainty. However, the condensation heat transfer on both samples are lower than on the Cu surface. According to the defined boundary condition (uniform surface temperature) the HTC will not depend on the bulk properties of the material such as thermal conductivity. However, the HTC will depend on the surface properties of the investigated material: surface roughness and surface energy.

Surface roughness has been shown to have an effect on the condensation HTC. According to Yun et al. [22], the roughness will cause an increase in the wall shear stress at the liquid-surface interface, which again results in a liquid retention on the surface and a thicker liquid film compared to on a smooth surface. A thicker film has a larger thermal resistance than a thinner film, and the HTC is therefore reduced.

As stated previously, the CO_2 film thickness may approach the same order of magnitude as the surface roughness when the subcooling is low. At a certain point, which is roughness and material dependent, the thermal resistance through the thin CO_2 film and through the roughness peaks will become similar. A simple parametric study shows that this occurs at a CO_2 thickness of 5.7μm for the steel surface and at 1.95μm for the Cu surface. Below these thicknesses, the temperature will no longer be uniform in the liquid–solid interface, and the values of HTC are undefined. This is reflected in the experimental data at low subcooling, where we see a large variation in the calculated HTCs.

In Fig. 14 it is shown that the theoretical liquid film thickness is

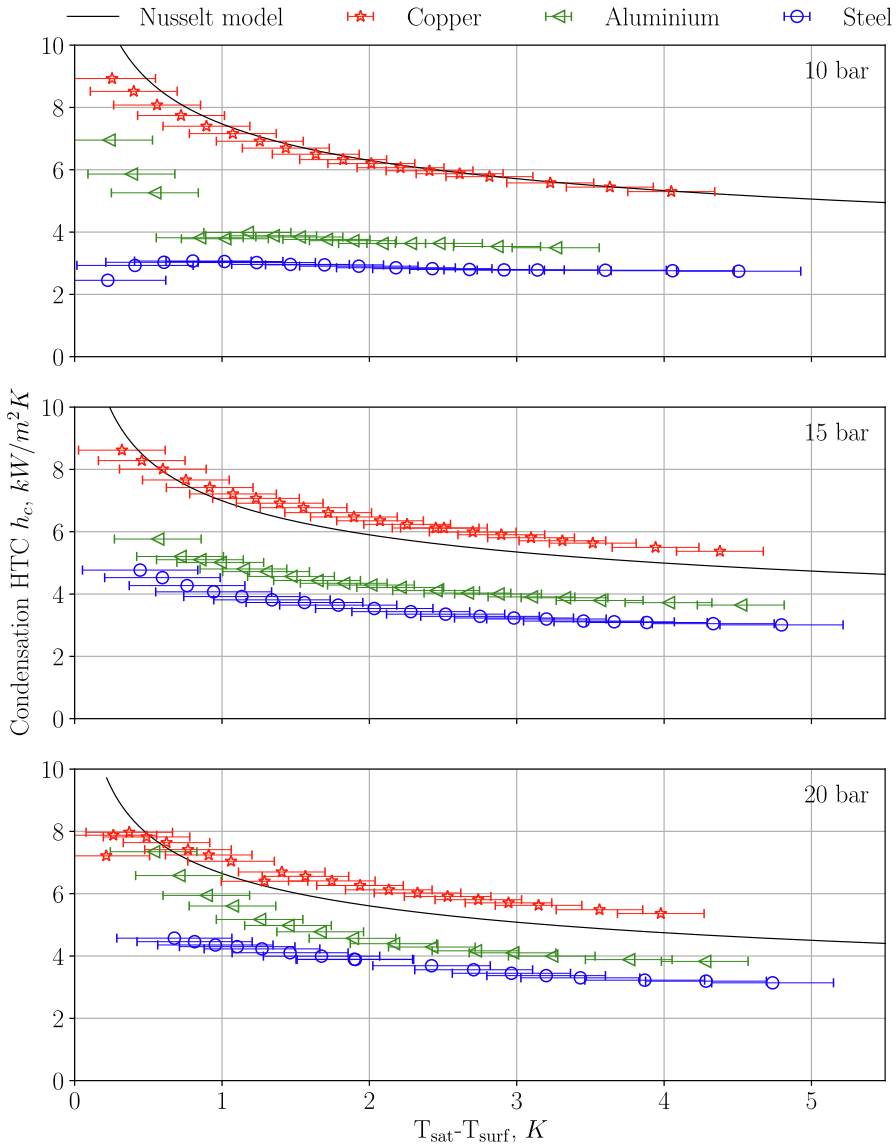

Fig. 10. Condensation HTC for Cu, Al, and steel at 10, 15 and 20 bar saturation pressure, respectively. The Nusselt models for the 15 bar and 20 bar saturation pressure are included for comparison, and a modified Nusselt model is presented.

lower for CO_2 than for water. Here, the Nusselt model is used to calculate the thickness. Assuming that the CO_2 film is thinner than a water film at the same level of surface subcooling, the effect of roughness will be more pronounced for CO_2 than for water, and we can expect larger deviations from the Nusselt model than reported for water.

Surface energy of a solid surface directly relates to the wetting properties of a liquid on the surface. A high surface energy is linked to a fully wetting surface at which a liquid spreads, while on a low surface energy solid, the liquid will form discrete droplets [39]. A material with high surface energy will, hence, adhere more strongly to a liquid than a material with low surface energy. Even though no droplets are observed in this work, it is reasonable to assume that the difference in surface energy between the samples will influence the liquid adhesion, and therefore retention on the surface. The surface energy of the materials in this work, presented in Table 2, are in three different orders of magnitude, with Cu highest and steel lowest. According to theory the Cu will adhere more to CO_2 than Al and steel and a lower HTC is therefore expected on Cu, if surface energy was the only effect. The difference in heat transfer on the three samples is therefore attributed to a combination of surface roughness and surface energy. A low surface roughness and a high surface energy, which is the case for the Cu sample, could according to the mentioned mechanisms, result in either a higher or lower HTC depending on the relative effect of the surface properties. A quantification of the relative effect will require additional experiments on a larger set of samples with different surface energies and roughnesses to decipher. However, the results indicate that the roughness has the highest impact on the heat transfer and that a thicker liquid film due to roughness induced retention results in a lower HTC on the Al and steel samples.

4.5. CO_2 adsorption on Cu

When conducting the experiments on Cu, we observed that the experimental HTC gradually decreased for consecutive experiments at the same conditions. Fig. 15 shows the results from five repeated experiments on the same Cu sample, conducted at five different days. The difference between the highest and lowest results at subcooling of 3k is about $6 kWm^{-2}$. An investigation on CO_2 impact on Cu revealed that the Cu surface is altered by CO_2 due to adsorption on the surface. When creating products out of captured CO_2, or when adsorbing CO_2 from a

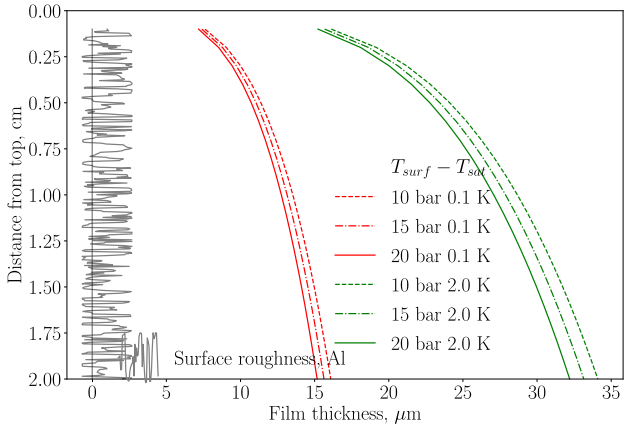

Fig. 11. The film thickness as predicted by the Nusselt model is shown for saturation pressures of 10 bar, 15 bar and 20 bar, and for 0.1k and 2.0k subcooling. The magnitude of the roughness on Al (the most rough surface) is represented by a random line with amplitude as the Peak-to-valley roughness = 2μm.

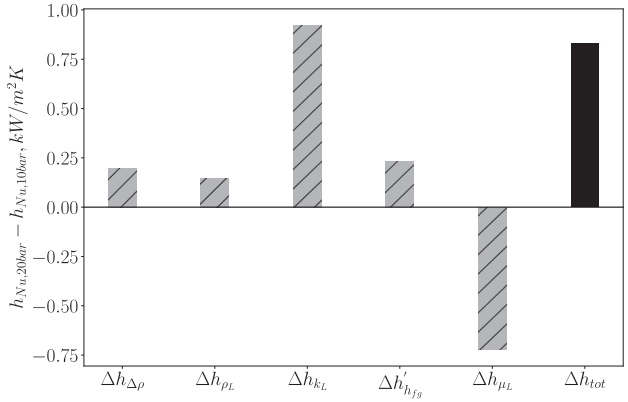

Fig. 12. The individual contributions of the change in condensate properties to the difference in h_{Nu} according to the Nusselt model. The total change in h_{Nu} when the saturation pressure is increased from 10 bar to 20 bar is the shown in solid black.

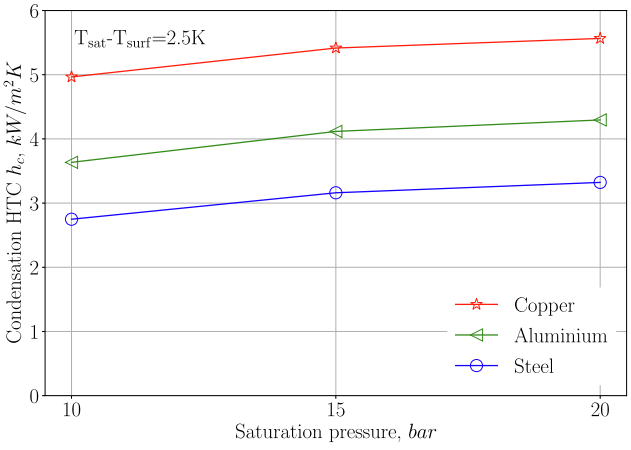

Fig. 13. Condensation HTC as a function of saturation pressure for Cu, Al, and Stainless steel at 2.5k subcooling.

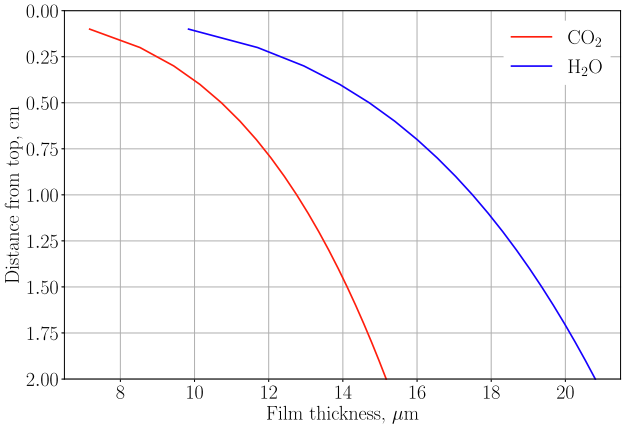

Fig. 14. The film thickness of H_2O and CO_2 on a vertical surface calculated with Nusselt theory (Eq. (6)). The subcooling is 0.1k in both cases. The average difference between the film thicknesses. is 4.6μm.

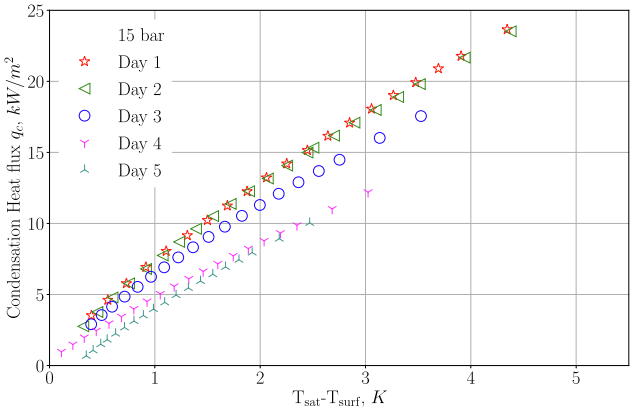

Fig. 15. Condensation heat flux for Cu at 15 bar saturation pressure, recorded at five different days, with equal settings.

gas, Cu is often used as a catalyst for CO_2 dissociation. Hence, adsorption of CO_2 on Cu is a known phenomena, and could therefore be the cause of the decrease in the heat flux results on Cu in the consecutive experiments. Previous studies have concluded that CO_2 adsorption does not occur on undisturbed flat Cu surfaces [40,41,24]. Those studies investigated gaseous CO_2 at low temperatures, and liquid CO_2 adsorption is not mentioned. The results in the present work indicate a surface modification of the Cu after several repetitions of condensation, with the decrease of heat flux. The phenomenon must be investigated further in order to depict the mechanisms and determine the degree to which the HTC is reduced. A study of the chemical composition of the surface and the amount of adsorbed CO_2 would be especially interesting, e.g. by thermal desorption spectroscopy.

5. Conclusion and outlook

In this work, an experimental method to measure the heat transfer during condensation of CO_2 on various materials is developed and validated. The main features of the associated setup are a heat transfer Cu cylinder, a two-phase flow cooling element, providing temperatures down to −55 °C, and a pressure chamber constructed for pressures between 1 and 20 bar. With the experimental method, we have measured the condensation heat transfer of CO_2, and revealed an effect of the condenser surface properties. The condensation process has been investigated at three levels of saturation pressure: 10, 15, and 20 bar. The condensation heat flux and HTC increase with pressure, which is the

opposite to the behavior of the Nusselt model. This could be caused by the properties of CO_2 and especially how the viscosity changes with pressure. The three commonly used process equipment materials, Cu, Al, and Stainless steel (316) have been investigated and the condensation HTC was presented. The results show that the heat flux and HTC are highest when condensing CO_2 on Cu, and are lowest on Al and steel. We propose that the difference is caused by the variation in surface roughness and surface energy between the three materials. A high surface roughness leads to liquid retention and therefore a higher liquid film thickness on the surface. A high liquid thickness is related to high thermal resistance and hence a low heat transfer coefficient. The surface property dependency is, however, not fully understood and a further investigation is needed. We suggest, for instance, to do a parametric study of surface roughness and surface energy separately, e.g. by fabricating a number of Cu, Al and steel surfaces with a variety of roughnesses. In such a way a correlation of the surface properties and the condensation HTC can be developed. We also suggest to investigate further the condensation heat transfer at low subcooling (below 1k) and at low saturation pressures, as the deviation between experiments and models are particularly large for these parameters. In addition, the film thickness is an important parameter for the filmwise condensation heat transfer, and the actual film thickness of the condensate as a function of saturation pressure and subcooling should be investigated further through measurements and simulations. Finally, we suggest to conduct a study on liquid CO_2 adsorption on Cu, for example by thermal desorption spectroscopy, as the results indicate that the Cu surface is altered by the CO_2 condensate.

Declaration of Competing Interest

The authors declare that they have no known competing financial interests or personal relationships that could have appeared to influence the work reported in this paper.

Acknowledgements

This publication has been produced with the support of the Research Council of Norway through the CLIMIT funding program (254813).

Appendix A. Supplementary material

Supplementary data associated with this article can be found, in the online version, at https://doi.org/10.1016/j.expthermflusci.2021.110440.

References

[1] S.K. Fischer, Total equivalent warming impact: a measure of the global warming impact of CFC alternatives in refrigerating equipment, Int. J. Refrig 16 (6) (1993) 423–428, https://doi.org/10.1016/0140-7007(93)90059-H.
[2] J. Pettersen, A. Hafner, G. Skaugen, H. Rekstad, Development of compact heat exchangers for co2 air-conditioning systems, Int. J. Refrig 21 (3) (1998) 180–193, https://doi.org/10.1016/S0140-7007(98)00013-9.
[3] C. Aprea, A. Maiorino, An experimental evaluation of the transcritical co2 refrigerator performances using an internal heat exchanger, Int. J. Refrig 31 (6) (2008) 1006–1011, https://doi.org/10.1016/j.ijrefrig.2007.12.016, http://www.sciencedirect.com/science/article/pii/S0140700708000030.
[4] Z.-B. Liu, Y.-L. He, Y.-F. Yang, J.-Y. Fei, Experimental study on heat transfer and pressure drop of supercritical co2 cooled in a large tube, Appl. Therm. Eng. 70 (1) (2014) 307–315, https://doi.org/10.1016/j.applthermaleng.2014.05.024.
[5] I.E. Agency, Energy technology roadmap 2017, International Energy Agency (2017) 393.
[6] A. Alabdulkarem, Y. Hwang, R. Radermacher, Development of CO2 liquefaction cycles for co2 sequestration, Appl. Therm. Eng. 33–34 (2012) 144–156, https://doi.org/10.1016/j.applthermaleng.2011.09.027.
[7] A. Aspelund, M.J. Mølnvik, G. De Koeijer, Ship transport of CO2, Chem. Eng. Res. Des. 84 (9) (2006) 847–855, https://doi.org/10.1205/cherd.5147.
[8] S. Roussanaly, G. Skaugen, A. Aasen, J. Jakobsen, L. Vesely, Techno-economic evaluation of CO2 transport from a lignite-fired igcc plant in the czech republic, Int. J. Greenhouse Gas Control 65 (2017) 235–250, https://doi.org/10.1016/j.ijggc.2017.08.022.
[9] L. Gao, M. Fang, H. Li, J. Hetland, Cost analysis of CO2 transportation: Case study in china, Energy Procedia 4 (2011) 5974–5981, https://doi.org/10.1016/j.egypro.2011.02.600.
[10] F. Neele, R. de Kler, M. Nienoord, P. Brownsort, J. Koornneef, S. Belfroid, L. Peters, A. van Wijhe, D. Loeve, CO2 transport by ship- the way forward in europe, in: 13th International Conference on Greenhouse Gas Control Technologies, GHGT-13, Vol. 114, Energy Procedia, 2017, pp. 6824–6834. doi:10.1016/j.egypro.2017.03.1813. doi: 10.1016/j.egypro.2017.03.1813.
[11] Z. Zhang, Z.L. Weng, T.X. Li, Z.C. Huang, X.H. Sun, Z.H. He, J. Van Es, A. Pauw, E. Laudi, R. Battiston, CO2 condensation heat transfer coefficient and pressure drop in a mini-channel space condenser, Exp. Thermal Fluid Sci. 44 (2013) 356–363, https://doi.org/10.1016/j.expthermflusci.2012.07.007.
[12] J. Heo, H. Park, R. Yun, Condensation heat transfer and pressure drop characteristics of CO2 in a microchannel, Int. J. Refrig 36 (6) (2013) 1657–1668, https://doi.org/10.1016/j.ijrefrig.2013.05.008.
[13] P. Li, S. Norris, Heat transfer correlations for co2 flowing condensation in a tube at low temperatures, Appl. Therm. Eng. 93 (2016) 872–883, https://doi.org/10.1016/j.applthermaleng.2015.09.072.
[14] M.M. Shah, Prediction of heat transfer during condensation of carbon dioxide in channels, Appl. Therm. Eng. 93 (2016) 192–199, https://doi.org/10.1016/j.applthermaleng.2015.09.016.
[15] P. Li, J.J.J. Chen, S. Norris, Flow condensation heat transfer of CO2 in a horizontal tube at low temperatures, Appl. Therm. Eng. 130 (2018) 561–570, https://doi.org/10.1016/j.applthermaleng.2017.11.004.
[16] W. Nusselt, Die oberflachen kondensation des wasserdamfes, Zeitschrift des Vereines Deutscher Ingenieure 60 (1916) 541–569.
[17] F.P. Incropera, D.P. DeWitt, T.L. Bergman, A.S. Lavine, Fundamentals of Heat and Mass Transfer, 6th Edition, John Wiley & Sons, 2007.
[18] S.H. Hoenig, S. Modak, Z. Chen, M. Kaviany, J.F. Gilchrist, R.W. Bonner, Role of substrate thermal conductivity and vapor pressure in dropwise condensation, Appl. Therm. Eng. 178 (2020) 115529, https://doi.org/10.1016/j.applthermaleng.2020.115529.
[19] J. Zhang, X. Zhu, M.E. Mondejar, F. Haglind, A review of heat transfer enhancement techniques in plate heat exchangers, Renew. Sustain. Energy Rev. 101 (2019) 305–328, https://doi.org/10.1016/j.rser.2018.11.017.
[20] J. Soontarapiromsook, O. Mahian, A.S. Dalkilic, S. Wongwises, Effect of surface roughness on the condensation of R-134a in vertical chevron gasketed plate heat exchangers, Exp. Thermal Fluid Sci. 91 (2018) 54–63, https://doi.org/10.1016/j.expthermflusci.2017.09.015.
[21] K. Nilpueng, S. Wongwises, Experimental study of single-phase heat transfer and pressure drop inside a plate heat exchanger with a rough surface, Exp. Thermal Fluid Sci. 68 (2015) 268–275, https://doi.org/10.1016/j.expthermflusci.2015.04.009.
[22] R. Yun, J. Heo, Y. Kim, Effects of surface roughness and tube materials on the filmwise condensation heat transfer coefficient at low heat transfer rates, Int. Commun. Heat Mass Transfer 33 (4) (2006) 445–450, https://doi.org/10.1016/j.icheatmasstransfer.2006.01.009.
[23] F. Solymosi, The bonding, structure and reactions of CO2 adsorbed on clean and promoted metal surfaces, J. Mol. Catal. 65 (3) (1991) 337–358, https://doi.org/10.1016/0304-5102(91)85070-I.
[24] F. Muttaqien, Y. Hamamoto, K. Inagaki, Y. Morikawa, Dissociative adsorption of CO2 on flat, stepped, and kinked Cu surfaces, J. Chem. Phys. 141 (3) (2014) 034702, https://doi.org/10.1063/1.4887362.
[25] C.J. Geankoplis, Transport Processes and Separation Process Principles, 4th Edition, Prentice Hall, 2003.
[26] D.J. Preston, K.L. Wilke, Z. Lu, S.S. Cruz, Y. Zhao, L.L. Becerra, E.N. Wang, Gravitationally driven wicking for enhanced condensation heat transfer, Langmuir 34 (15) (2018) 4658–4664, https://doi.org/10.1021/acs.langmuir.7b04203.
[27] C.-Y. Wang, C.-J. Tu, Effects of non-condensable gas on laminar film condensation in a vertical tube, Int. J. Heat Mass Transf. 31 (11) (1988) 2339–2345, https://doi.org/10.1016/0017-9310(88)90165-2.
[28] X.-H. Ma, X.-D. Zhou, Z. Lan, Y.-M. Li, Y. Zhang, Condensation heat transfer enhancement in the presence of non-condensable gas using the interfacial effect of dropwise condensation, Int. J. Heat Mass Transf. 51 (7–8) (2008) 1728–1737, https://doi.org/10.1016/j.ijheatmasstransfer.2007.07.021.
[29] X.M. Wu, T. Li, Q. Li, F. Chu, Approximate equations for film condensation in the presence of non-condensable gases, Int. Commun. Heat Mass Transfer 85 (2017) 124–130, https://doi.org/10.1016/j.icheatmasstransfer.2017.05.007.
[30] R. Span, W. Wagner, A new equation of state for carbon dioxide covering the fluid region from the triple-point temperature to 1100 k at pressures up to 800 mpa, J. Phys. Chem. Ref. Data 25 (6) (1996) 1509–1596, https://doi.org/10.1063/1.555991.
[31] National Institute of Standards and Technology (2018). [link]. https://webbook.nist.gov/chemistry/fluid/.
[32] S.I. Abu-Eishah, Correlations for the thermal conductivity of metals as a function of temperature, Int. J. Thermophys. 22 (6) (2001) 1855–1868, https://doi.org/10.1023/A:1013155404019.
[33] Z. Jian-Min, M. Fei, X. Ke-Wei, Calculation of the surface energy of fcc metals with modified embedded-atom method, Chin. Phys. 13 (7) (2004) 1082–1090, https://doi.org/10.1088/1009-1963/13/7/020.
[34] A. Kinloch, Adhesion and Adhesives, Springer Netherlands, 1987. doi:10.1007/978-94-015-7764-9.
[35] O. Santos, T. Nylander, R. Rosmaninho, G. Rizzo, S. Yiantsios, N. Andritsos, A. Karabelas, H. Muller-Steinhagen, L. Melo, L. Boulange-Petermann, C. Gabet, A. Braem, C. Traegaardh, M. Paulsson, Modified stainless steel surfaces targeted to

reduce fouling–surface characterization, J. Food Eng. 64 (1) (2004) 63–79, https://doi.org/10.1016/j.jfoodeng.2003.09.013.
[36] Q. Baojin, Z. Li, X. Hong, S. Yan, Experimental study on condensation heat transfer of steam on vertical titanium plates with different surface energies, Exp. Thermal Fluid Sci. 35 (1) (2011) 211–218, https://doi.org/10.1016/j.expthermflusci.2010.09.003.
[37] W.M. Rohsenow, Heat transfer and temperature distribution in laminar film condensation, Transactions ASME 78 (1956) 1645–1648.
[38] H. Akimoto, Y. Anoda, K. Takase, H. Yoshida, H. Tamai, Condensation Heat Transfer, Springer Japan (2016) 347–359, https://doi.org/10.1007/978-4-431-55603-9_17.
[39] J. Wu, s. Ervik, I. Snustad, S. Xiao, A. Brunsvold, J. He, Z. Zhang, Contact angle and condensation of a co2 droplet on a solid surface, The Journal of Physical Chemistry C 123 (1) (2019) 443–451. doi:10.1021/acs.jpcc.8b08927. doi: 10.1021/acs.jpcc.8b08927.
[40] J. Nakamura, J.A. Rodriguez, C.T. Campbell, Does CO2 dissociatively adsorb on cu surfaces? J. Phys.: Condens. Matter 1 (1989) https://doi.org/10.1088/0953-8984.SB149–SB160.
[41] I.A. Boenicke, W. Kirstein, F. Thieme, A study on CO2 dissociation on a stepped (332) copper surface, Surf. Sci. 307–309 (1994) 177–181, https://doi.org/10.1016/0039-6028(94)90390-5.